Cell Reports

Article

Structural changes in chromosomes driven by multiple condensin motors during mitosis

Graphical abstract

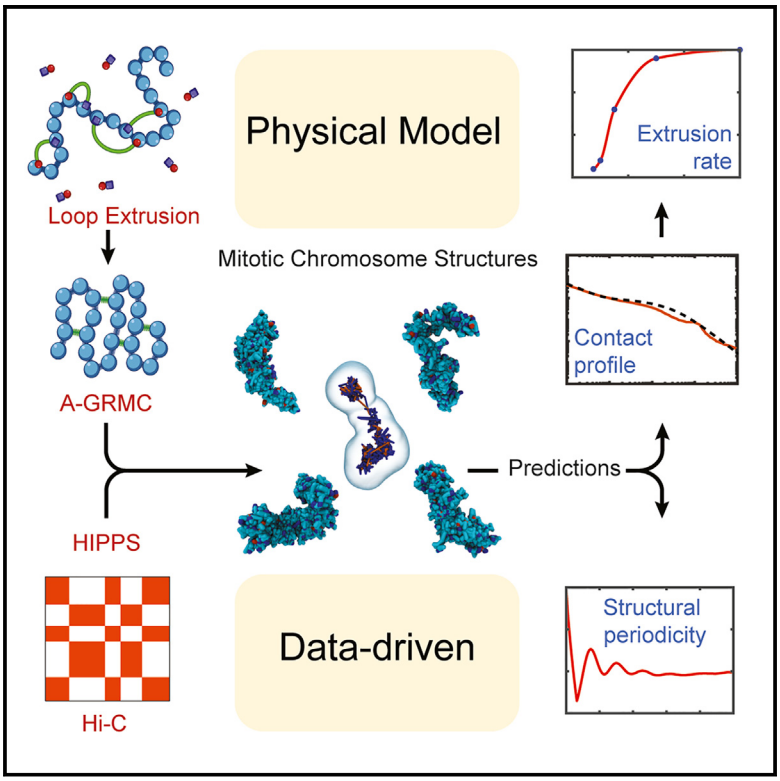

Authors

Atreya Dey, Guang Shi, Ryota Takaki, D. Thirumalai

Correspondence

dave.thirumalai@gmail.com

In brief

Multiple condensin motors drive structural changes in chromosomes during mitosis. Dey et al. create a theoretical model to quantitatively predict these structures. The theory and a data-driven model quantitatively predict the experimental observations for two cell lines. The handedness of the helical mitotic structures changes randomly along the helical axis.

Highlights

- Active polymer model accounts for chromosome organization through mitosis
- Asymmetric loop extrusion by condensin motors describes mitotic structures
- Mitotic chromosome structures are helical with a dynamically changing helix axis
- Helical structures have random changes in handedness along the helical scaffold

Dey et al., 2023, Cell Reports *42*, 112348
April 25, 2023
https://doi.org/10.1016/j.celrep.2023.112348

CellPress

Cell Reports

CellPress
OPEN ACCESS

Article

Structural changes in chromosomes driven by multiple condensin motors during mitosis

Atreya Dey,[1] Guang Shi,[2] Ryota Takaki,[3] and D. Thirumalai[1,4,5,*]
[1]Department of Chemistry, The University of Texas at Austin, Austin, TX 78712, USA
[2]Department of Materials Science, University of Illinois, Urbana, IL 61801, USA
[3]Max Planck Institute for the Physics of Complex Systems, Nöthnitzer Str.38, 01187 Dresden, Saxony, Germany
[4]Department of Physics, The University of Texas at Austin, Austin, TX 78712, USA
[5]Lead contact
*Correspondence: dave.thirumalai@gmail.com
https://doi.org/10.1016/j.celrep.2023.112348

SUMMARY

We create a computational framework that utilizes loop extrusion (LE) by multiple condensin I/II motors to predict changes in chromosome organization during mitosis. The theory accurately reproduces the experimental contact probability profiles for the mitotic chromosomes in HeLa and DT40 cells. The LE rate is smaller at the start of mitosis and increases as the cells approach metaphase. Condensin II-mediated mean loop size is about six times larger than loops because of condensin I. The loops, which overlap each other, are stapled to a central dynamically changing helical scaffold formed by the motors during the LE process. A polymer physics-based data-driven method that uses the Hi-C contact map as the only input shows that the helix is characterized as random helix perversions (RHPs) in which the handedness changes randomly along the scaffold. The theoretical predictions, which are testable using imaging experiments, do not contain any parameters.

INTRODUCTION

Over the last decade, a variety of experimental tools have been developed, which have yielded unprecedented glimpses of the nuclear architecture. These methods fall under the rubric of chromosome conformation capture techniques (3C, 4C, 5C, Hi-C, and Micro-C).[1–6] The output from a typical Hi-C experiment is extraction of the average contact map (CM), a matrix whose elements give the relative probability that two loci, separated by the genomic distance (s), are in spatial proximity. Although there are nuances in the organization of the genomes, the CMs reveal that there are at least two major length scales that characterize the structures of mammalian interphase chromosomes. Depending on the resolution of the Hi-C experiments, on scales of a kilobase pair to a megabase pair, active (euchromatin) and inactive (heterochromatin) loci undergo microphase separation[7–10] into two compartments, which are manifested as checkerboard patterns in the ensemble-averaged CMs.[4] On a smaller length scale, there are fine structures in the CMs that are referred to as topologically associating domains (TADs).[2]

As a cell transitions from interphase to mitosis, chromosome structures change dramatically. The distinct separation between euchromatin and heterochromatin that is prominent in interphase breaks down, and chromosomes become compact, adopting a characteristic rod-like or cylindrical shape.[11–18] For a comprehensive overview of mitotic chromosomes, we refer the reader to a recent review.[19] In an insightful study,[20] Hi-C experiments were performed to monitor the changes in chicken DT40 cells as the cells transitioned from G2 to mitotic phase. By building on earlier studies,[21–30] the authors showed that the changes in organization in the chicken DT40 genome are driven by ATPase motors, condensin I and condensin II. The major findings of this study are as follows. (1) Less than 10 min after the cells enter prophase, signatures of compartment formation as well as the characteristics of TADs are lost. (2) In the time window 10 min $\leq t \leq$ 60 min, the most prominent feature in the contact probability $P(s)$ as a function of the genomic distance (s) between two loci is the emergence of a peak whose location shifts to higher s values as the cell cycle progress (see Figure 3A in Gibcus et al.[20]). (3) By successively depleting condensin II (CAP-H2-mAID in Figure 5A in Gibcus et al.[20]) and condensin I (CAP-H-mAID in Figure 5A in Gibcus et al.[20]), it was suggested that the presence of the peak and its movement to higher s values is due to the emergence of a helical scaffold. Moreover, the authors argued that formation of the helical structure is largely driven by the condensin II motor, with condensin I playing little or no role. Informed by the experimental observations,[17,31–33] they also performed polymer simulations in which chromosomes were artificially confined to a cylinder and forced to adopt a static helical scaffold from which non-overlapping loops emanated. The parameters in the polymer model were adjusted to reproduce the observed $P(s)$ versus s extracted from the Hi-C map.

That the structures of the mitotic chromosome are likely to be helical was proposed long ago.[15,17,34–39] However, the physical mechanisms that drive helix formation are not evident from Hi-C[20] or from the more recent imaging experiments.[40] In particular, there is no understanding of the roles played by multiple copies

of the two motor proteins (condensin I and II) in shaping the chromosome structures during mitosis. This is a difficult problem to solve because a large number of motors (see supplemental information for an estimate of the number of motors) are involved in the loop extrusion (LE) process. Their structures and ATPase cycles (even for single condensin motors) have not been fully elucidated. A potential clue regarding how to proceed comes from several single-molecule experiments[41,42], which have not only measured the speed of LE but have also shown that a single condensin molecule extrudes loops in a one-sided asymmetric manner or two-sided symmetric fashion. The single-molecule studies set the stage for our theoretical investigations of the mitotic chromosome architecture involving multiple motors and how it changes as the cell cycle progress.

To explain the experimental results, we first generalized the theory developed by Takaki et al.[43] for LE for a single motor to multiple motors (details are given in STAR Methods) to determine the changes in the organization of chromosomes as the cell progresses through different stages of the mitosis cycle. The extruded loops were then used in a polymer model that is based on the generalized Rouse model for chromosomes (GRMC).[44–46] The resulting active GRMC (A-GRMC) model without any adjustable parameter shows that asymmetric LE alone can create mitotic chromosome structures, observed in HeLa and DT40 cells.[20,47]

To reproduce $P(s)$ at various time points (t = 7.5, 10, 15 and 30 min) in the cell cycle of the condensin II-depleted chicken DT40 cells, we found that it was necessary to vary the step sizes taken by the motor. The A-GRMC does not quantitatively account for the dependence of $P(s)$ on s for the condensin I-depleted DT40 cells, which suggests that the coordinated action of condensin II motors in generating long loops has to differ from condensin I, which generates shorter loops on an average. To complement the A-GRMC predictions, we calculated the three-dimensional (3D) structures of the chromosomes throughout the cell cycle for DT40 cells using the Hi-C-polymer-physics-structures (HIPPS) method.[48] The calculated $P(s)$ using the predicted 3D structures agree quantitatively with the experimental data at all times. By computing the angular correlation function using the calculated structures, we show that the helical conformations emerge naturally as the cells transition to the mitotic phase. The 3D structures suggest that the loops in the mitotic chromosomes are arranged around a helical scaffold, which changes from one realization to another. The helical regions randomly alternate in chirality, suggestive of random helix (or tendril) perversion (RHP). Through a combination of the A-GRMC theory and the calculated 3D structures using the HIPPS method, we account nearly quantitatively for many (if not all) aspects of the structural changes in chromosomes during mitosis.

RESULTS

A-GRMC calculations quantitatively reproduce $P(s)$ for mitotic chromosomes

The theory for LE by multiple condensin motors is based on the mechanism sketched in Figure 1. The physical picture relies on the scrunching mechanism,[43,49] which assumes that the heads of the motors that are bound to the DNA are relatively immobile, whereas the hinge moves toward the stationary heads during the catalytic cycle. Loops are extruded by repeated transition of the hinge toward the motor heads through an asymmetric allosteric LE mechanism.[43] The parameters needed for the A-GRMC simulations (Table S5) are either taken or inferred from experiments (see details in the STAR Methods). The experimental data are shown in Tables S1–S4). Figure 2A shows a snapshot of the loop conformation generated by multiple motors in a 10-Mbp chromosome (also shown in Video S2). The helix-like scaffold is generated by the motor proteins to which the loops are stapled. We find evidence of Z loops and nested loops (Figure 2B) in the stochastic kinetic simulations based on A-GRMC. The loops, extruded by condensin I, are, on an average, smaller in size compared with the ones generated by condensin II (Figure 2C, Video S1). Because the linear density of condensin I is greater than condensin II, the loops extruded by the former resemble a dense polymer brush-like structure. On the other hand, loops generated by condensin II are fewer in number but longer, which facilitates formation of long-range contacts between the loci. It is worth pointing out that the helical scaffold and, hence, the structures of the mitotic chromosomes vary from one realization to another. The A-GRMC simulations also show that the majority of the loops are nested and are interspersed with a smaller fraction of Z-loops (Figure 2D). The actual numbers are shown in Figure S3. Finally, the calculations using the scrunching mechanism quantitatively account for the dependence of $P(s)$ on s for HeLa cells and DT40 cells (Figure 2E). The results in Figure 2 provide a mechanistic basis for generating the dynamical helical scaffold created by multiple condensin motors in the two cell types.

Symmetric LE

It has been suggested[41] that LE by a single yeast condensin motor is strictly asymmetric. In contrast, a more recent study[42] claims that LE by human condensin could be symmetric and asymmetric. Both mechanisms might be operative in *Xenopus* eggs.[50] It is possible that LE is mostly asymmetric during metaphase and symmetric during interphase.[51] To reconcile, at least partially, these seemingly opposing conclusions, we altered the LE scheme to investigate the consequences of symmetric LE on $P(s)$ as a function of s. As shown in Figure 3A, we randomly exchanged the mobile and static sites to allow a loop to form and grow on both sides. This is achieved by randomly switching the mobile and static sites with each other. If the probability of switching is equal, then a loop could grow on both sides, thus creating symmetric extrusion. In Figures 3B and 3C, we show two possible mechanisms for symmetric LE within the scrunching mechanism. Figure 3B illustrates that the loop itself is held between the two heads, while the hinge randomly binds to either side of the loop, resulting in symmetric LE. In Figure 3C, the loop is held at one of the two heads, and the hinge binds and reels in DNA from the opposite side. In this scenario, condensin has to shuttle the loop back and forth between the two heads, creating an effective symmetric extrusion. Experiments could be designed to assess the validity of either of the mechanisms. We find that fully symmetric extrusion and asymmetric extrusion result in the same $P(s)$ versus s (Figure 3D).

HeLa cells

Figure 3D shows that asymmetric extrusion coupled with natural formation of Z-loops and nested loops using the A-GRMC

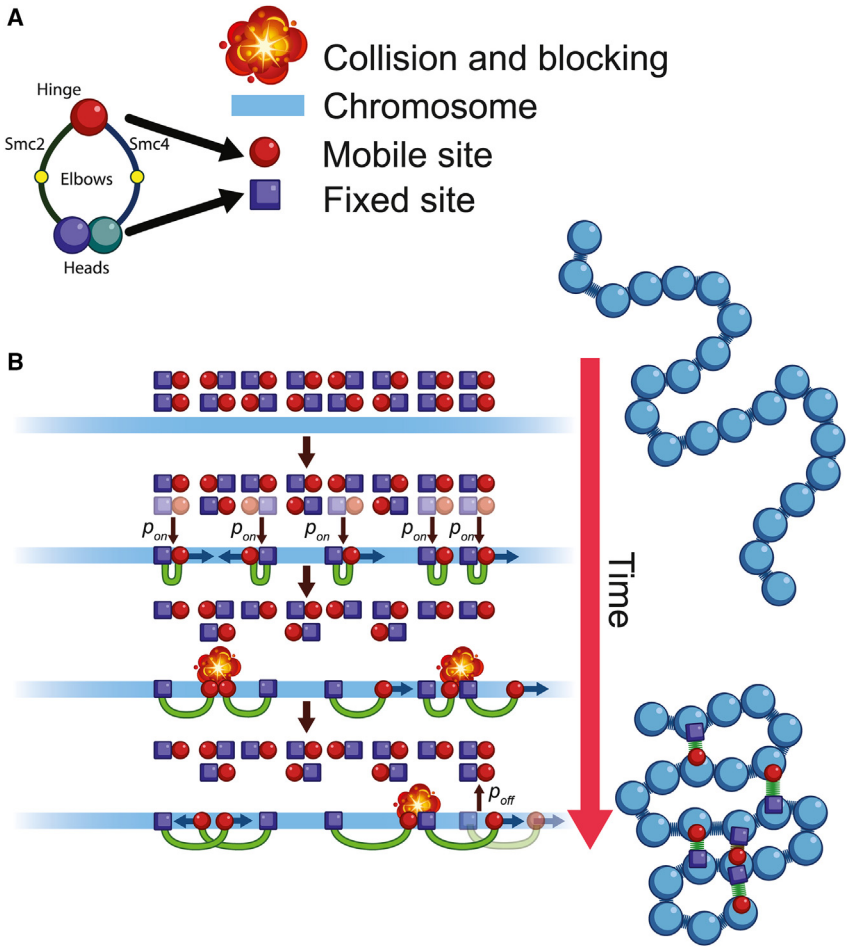

Figure 1. Mechanism of multiple-condensin-driven LE using A-GRMC

(A) Schematic of the structural features of a condensin (I or II) motor. The representation of the fixed sites (heads) and mobile sites (hinge) is based on the scrunching mechanism. The mobile and static sites of condensin are shown as red circles and blue squares, respectively.

(B) The dark blue arrows show the direction of LE by condensin. The green semicircle represents the extruded loop. Condensin motors bind to DNA with probability p_{on} and unbind with probability p_{off}, shown with black arrows. The mobile site takes a step (shown with small blue arrows) with probability P_{step} at each time step. When the motor stops, loops are extruded unidirectionally with a step size that is sampled from Equation 4. Only the mobile site moves along the DNA. The movement is paused for $\tau_p = 7$ s when the motor encounters another site (mobile or static). The chromosome, which is divided into 10-kbp monomers, is shown in blue. Adjacent loci are linked by harmonic springs, and looped loci are connected by harmonic springs as well (green). The mobile and static heads of condensin are shown as red circles and squares, respectively.

simulations also reproduces mitotic chromosome structures in HeLa cells.[47] As shown in Table S5, a 100-Mbp HeLa cell chromosome has ≈343 condensin II and ≈2,553 condensin I molecules, as calculated based on experimental measurements (STAR Methods). Of these, on an average, ≈ 210 condensin II and ≈1205 condensin I molecules are bound to the chromosome. Of 1,415 bound condensin molecules, ≈ 97% are involved in one or more nested loops, and ≈ 45% participate in one or more Z-loops. These results show that overlapping loops and Z-loops ensure that the loops generated by multiple motors densely cover the entire chromosome without gaps.

Time-dependent changes in the mean loop length

The dependence of the average loop size changes as a function of time. Figure 4A shows that the loop sizes, averaged over 500 LE realizations, increase rapidly and saturate to a fixed value. The individual traces of the average loop sizes for five realizations reveal little change from one initial condition to another (Figure 4B). The average size of the loops generated by condensin I (≈ 250 kbp) is about six times smaller (Figure 4A) than those generated by condensin II (≈1,500 kbp). The long-range contacts established by condensin II motors likely stabilize the helical scaffold, whereas the preponderance of short-range contacts, driven by condensin I, are responsible for overall compaction. Similarly, it takes longer (by about an order of magnitude) for condensin II to extrude a long loop, even though the LE velocity is the same for the two types of motors.

Comparison of the calculated $P(s)$ as a function of s with experiments, with only condensin I at $t = 60$ min (Figure 4C), shows reasonable agreement. The decay of $P(s)$ occurs in two steps. On the scale $s \leq 1Mbp$ s, coinciding roughly with the size of the TADs, we find that $P(s) \sim s^{-0.7}$, whereas $P(s) \sim s^{-3/2}$ for $s > 1$Mbp. The values of the two exponents, calculated using the A-GRMC theory, are in reasonable agreement with experiments. Fits to the experimental $P(s)$ versus s (Figure 4C) yield $P(s) \sim s^{-0.5}$ ($s \leq 1Mbp$ s) and $P(s) \sim s^{-1.9}$ ($s > 1$Mbp). Although qualitatively similar, the agreement between our calculations and experiments for $P(s)$ in condensin I-depleted cells is less satisfactory for $s \leq 1Mbp$ s (Figure 4D). The CMs corresponding to Figures 4C and 4D are shown in Figure S7A. The calculated exponent and that extracted from the Hi-C data are 1.1 and 0.7, respectively. On scales greater than $s > 1$Mbp, the values of the exponent characterizing the decay of $P(s)$ coincide. Figures S2A and S2B show a comparison of the A-GRMC calculations with previous simulations from Gibcus et al.[20]

Effects of condensin I and condensin II depletion

Because condensin I and II are involved in mitotic chromosome formation, it is important to determine the differential contribution of the two motors in determining the dependence of $P(s)$ on s. It is known that condensin I and condensin II bind to chromosomes independently at different stages,[52,53] with the latter

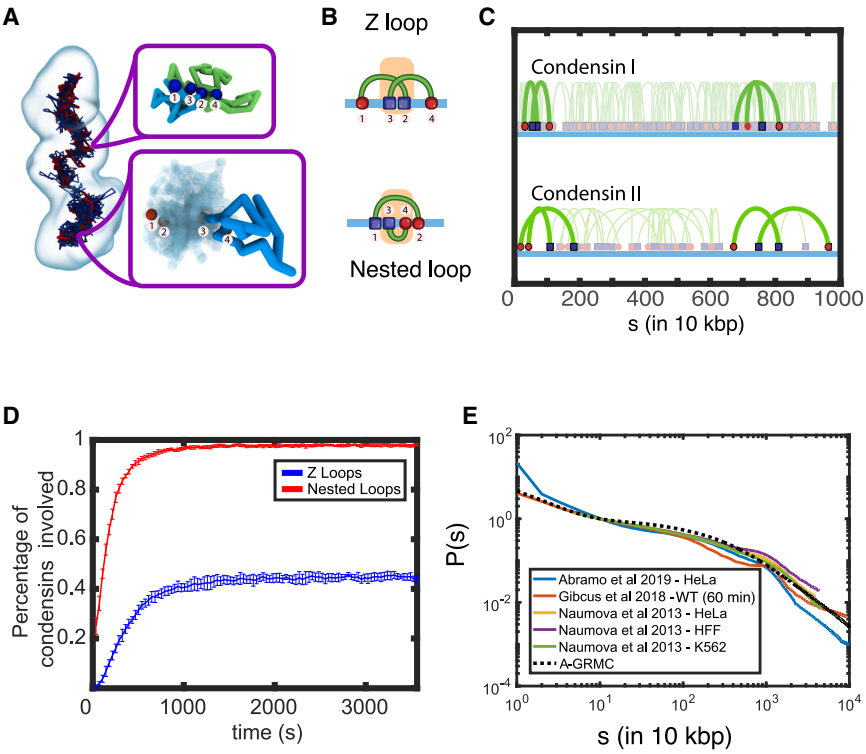

Figure 2. Loop generation mechanism

(A) A snapshot of a structure, generated in the A-GRMC simulations of the mitotic chromosomes, shows the backbone formed by the condensin molecules. Condensin I motors are shown in dark blue, whereas condensin II is shown in red. The magnified regions show an example of a Z-loop formed by two condensin I molecules and a nested loop formed by two condensin II molecules, respectively. For the Z-loop, the two loops are colored in cyan and green. For the nested loop, the larger loop is shown in transparent colors, while the smaller loop is shown in cyan.

(B) Cartoon depicting two condensin molecules involved in a Z-loop and a nested loop. The overlapping segment of the chromatin between each loop is highlighted.

(C) A snapshot of condensin I and II loops in 10 Mbp of DNA. Examples of the Z-loops and the nested loops in either condensin are highlighted.

(D) Fraction of condensin motors involved in formation of a Z-loop or nested loop as a function of time.

(E) $P(s)$ in the metaphase chromosomes from different experiments and cell types along with the predictions of the A-GRMC calculations (dashed lines). The A-GRMC calculations fall within the spread of the $P(s)$ in the experiments.

extruding larger loops because of the increased lifetime of the bound state (Figure 4A). The distinct roles played by condensin I and condensin II were examined by selectively depleting the two motors.[20] It was noticed that, when both motors are simultaneously present, there is a peak in the $P(s)$ in the DT40 chromosomes. The location of the peak moves to larger s values that is accompanied by an increase in the magnitude of $P(s)$ as the cell cycle proceeds toward mitosis. To determine the origin of the bump, the motors were selectively degraded, allowing them to infer $P(s)$ as a function of s in the presence of only one of the motors. An important experimental finding is that the bump in $P(s)$ is predominantly driven by condensin II, with condensin I playing little or no role. To assess the accuracy of the A-GRMC calculations, we calculated $P(s)$ by selectively depleting the condensin motors.

The results for condension II-depleted DT40 cells are shown in Figures 5A, 5C, and 5E. Using $P_{step} = 1$, there is reasonable agreement between the calculated and measured $P(s)$ as a function of s. We optimized the step size to obtain the smallest error between simulations and experiments. The values of the optimized P_{step} change with time (Figure 5A), which implies that the mean step size the motors take vary as mitosis progresses. The optimal values of P_{step} as a function of time are displayed in Figure 5C. Figure 5E shows that, at the optimized P_{step}, our theory quantitatively reproduces the measured[20] $P(s)$ curves at all times. Based on the results in Figure 5, we speculate that the variation in P_{step} implies that the mechanical tension along the chromosomes changes as cells progress to mitosis.

The results for condensin I-depleted cells are plotted in Figures 5B, 5D, and 5F. The results for $P(s)$ as a function of s, calculated at the optimum P_{step} values, are shown in Figure 5D; the errors between the calculated and experimental $P(s)$ are shown in Figure 5B. Although the agreement between theory and experiments is reasonable (Figure 5F), the simulations do not capture the prominent bump in the $P(s)$ when only condensin II is present. The bump in $P(s)$ is an indication of the underlying helical structure of mitotic chromosomes.[20] To obtain helical structures, the model must contain anisotropic interactions between the chromosomes and the motors. The absence of such interactions in the A-GRMC simulations explains the lack of the pronounced bump in $P(s)$ when condensin I is depleted.

Impact of the motor residence time, pausing time, and density of motors on $P(s)$

We explored the effects of changing the parameters in the A-GRMC on $P(s)$ as a function of s. The results are shown in Figure S4.

Lifetime of bound condensin motors

Figure S4A shows that increasing the residence time of condensin motors leads to additional long-range contacts, which is reflected in a plateau-like feature in $P(s)$ for $s > 10^5$ bp. As shown in Equation 2 in the STAR Methods, the unbinding probability of condensin molecules, p_{off}, is inversely proportional to the residence time. Thus, increasing the residence time decreases p_{off}, which, in turn, increases the lifetime of condensins that are bound to DNA. As a consequence, longer loops form, which enhance the $P(s)$ value at large s. A corollary of this finding is that the longer loops driven by condensin II are due to the enhanced residence time of condensin II ($\approx$6 min) on the chromosome compared with condensin I ($\approx$2 min).

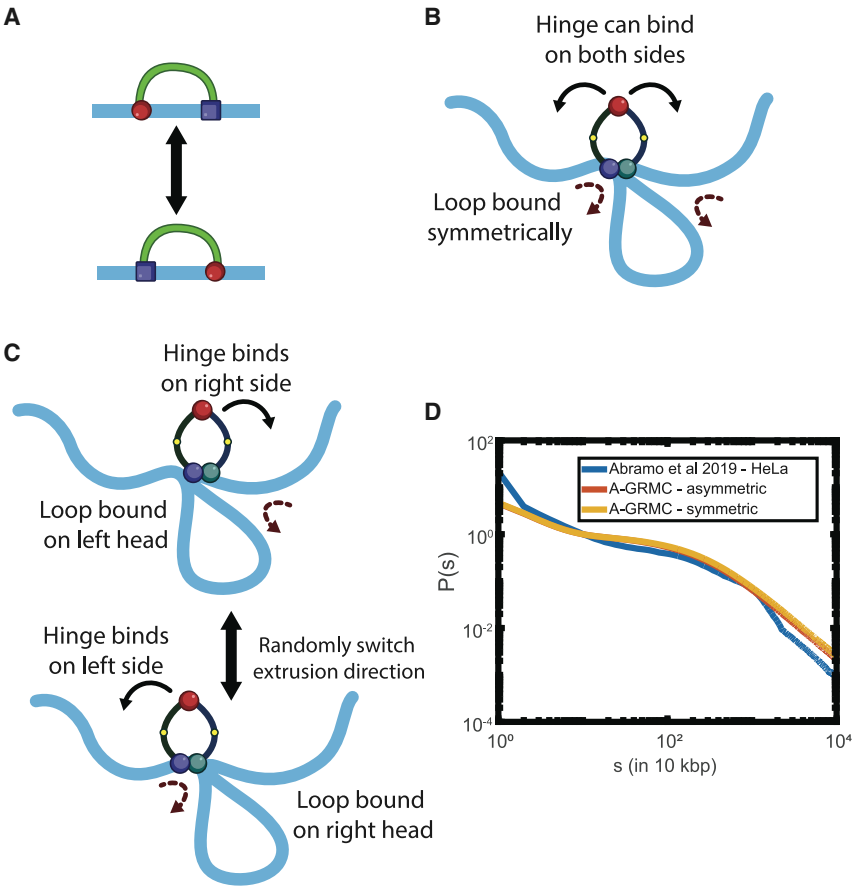

Figure 3. Symmetric versus asymmetric LE

(A) Symmetric extrusion is realized by exchanging the mobile and static sites (see also Figure 1). The cartoon shows possible mechanisms of symmetric extrusion according to the scrunching mechanism.

(B) The hinge can bind to both sides of the loop, and the loop is held between the two heads.

(C) The extrusion switches between two forms in the asymmetric extrusion.

(D) Data for $P(s)$ versus s for mitotic chromosomes for HeLa cells from experiments[47] compared with A-GRMC calculations using symmetric and asymmetric extrusion. Symmetric and asymmetric extrusion can reproduce the same $P(s)$ curves.

Pausing time

The effect of changing the pausing time, τ_p, has the opposite effect compared with increasing the residence time. Figure S4B shows that, upon increasing τ_p, the probability of contact formation for $s > 10^5$ bp sharply decreases. Comparison of the predicted and measured $P(s)$ shows that the optimal value of τ_p is about $4 \sim 8$ seconds. Our theory, therefore, could be used to extract the residence and the pausing times of condensin motors by fitting the predictions to the experimental $P(s)$ versus s.

Number of bound motors

The number of bound condensins (n_b) also influences the shape of the $P(s)$ curves, as shown in Figure S4C. Because $p_{on} \propto 1/(n_t/n_b - 1)$ (see Equation 3 in the STAR Methods), consequently increasing n_b while keeping n_t constant leads to a larger binding probability p_{on}. The increase in the density of bound condensins to DNA results in more loops being extruded. In addition, the values of $P(s)$ should be larger at large s values. However, when all available condensins are bound, the $P(s)$ does not change. The best fit to experiments shows that, on average, the number of bound condensins I is $N_b = 255$ (Figure S4C). We also calculated $P(s)$ by varying the p_{on}/p_{off} (Figure S4D), which is similar to changing $n_b/(n_t - n_b)$. Higher values of p_{on}/p_{off} result in more bound condensins, resulting in extrusion of longer loops.

Taken together, these results suggest that the biologically relevant parameters τ_p, τ_B, and n_b are optimized to extrude loops of appropriate sizes. It is likely that these parameters depend on the chromosomes and the cell type as well.

Helical structures of mitotic chromosomes are predicted using a data-driven method

To assess whether the bump in $P(s)$ could be reproduced and explained in terms of helical (or related) conformations, we used the HIPPS method.[48] As a complement to the A-GRMC simulations and to compare the extent of helix formation in DT40 and HeLa cells, we calculated $P(s)$ at different time points as the cell transitions from interphase to the mitotic phase using the HIPPS method, which predicts an ensemble of 3D chromosome structures with the measured Hi-C maps as the only input (STAR Methods).

The dependence of $P(s)$ on s for condensin I-depleted chromosomes in DT40 cells, calculated using the 3D structures, is in quantitative agreement (Figure 6A) with experiments at all times. In particular, the HIPPS method accounts for the pronounced peak (Figure 6B), which, as we show below, is important in producing structures with RHP. Naturally, the predictions are also quantitative for DT40 chromosomes when both motors are present (Figure 6C). It is also gratifying that the calculated and measured $P(s)$ for HeLa cells are also accurate (Figure 6D).

Periodicity in angular correlation functions

With the 3D coordinates of the loci at hand, we quantified the extent of helix formation at different times in the DT40 cell as it goes through the phases in the cell cycle. To this end, we used the angular correlation function

$$C(s) = \langle \mathbf{r}_{i,i+d} \cdot \mathbf{r}_{i+s,i+s+d} \rangle \qquad \text{(Equation 1)}$$

where $\mathbf{r}_{i,j}$ is the vector between the i^{th} and j^{th} loci, and $d = 32$[48]. For a perfect helix, $C(s)$ should be periodic, with a period that is proportional to the helical pitch (Figure S5). In Figure 7A, which shows $C(s)$ as a function of s at different times, upon condensin

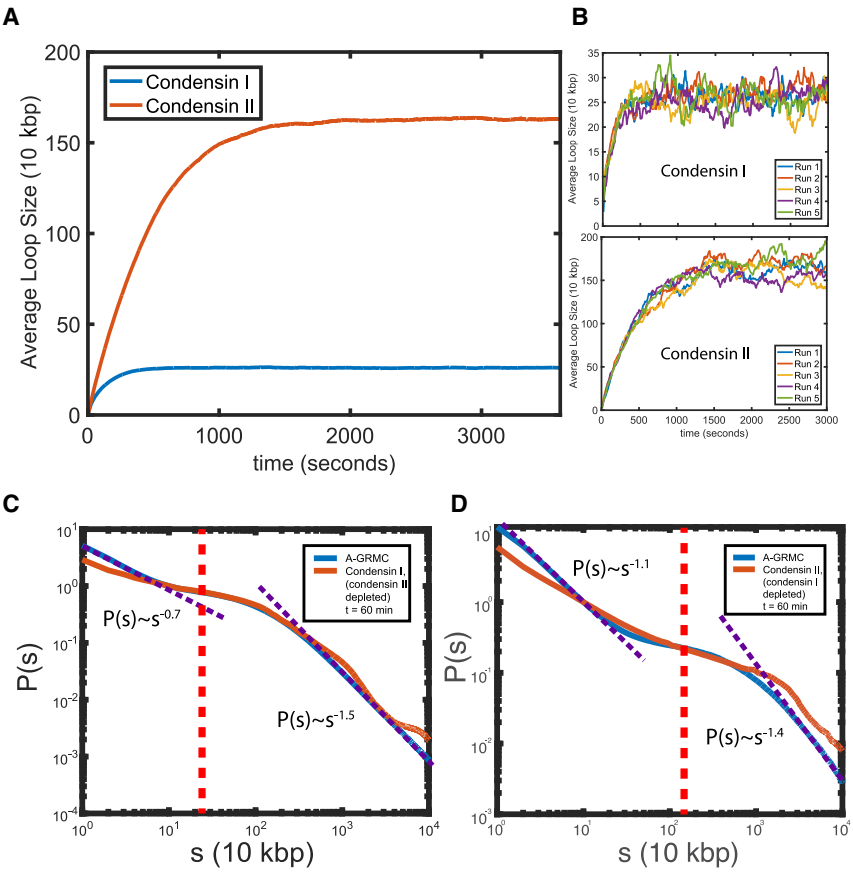

Figure 4. Time evolution of loop sizes and $P(s)$ curves for DT40 cells

(A) Average loop size as a function of time for condensin I without condensin II (blue) and condensin II without condensin I (red) from A-GRMC calculations. The mean loop sizes generated by condensin II are greater than the ones generated by condensin I even though the number of condensin I is larger than condensin II.

(B) Evolution of average loop size in 5 independent simulations for condensin I and II. The figure shows that the mean loop size is reached rapidly within 1,000 s after the extrusion process starts.

(C) Comparison of the dependence of $P(s)$ on s predicted by A-GRMC calculations and experiments at t = 60 min upon depletion of condensin II.

(D) $P(s)$ versus s for condensin I-depleted chromosomes at t = 60 min compared with the A-GRMC calculations. The red-dotted line indicates the average loop length.

(C) and (D) show a much sharper decrease in $P(s)$ when s exceeds the average loop length. The small and larger exponent values are calculated between 1 and 90 kbp and 10–100 Mbp, respectively.

II depletion, we see that there are small but discernible peaks at t = 15, 30 and 60 min. The locations of the peaks change from $s \approx 2.5$ Mbp (t = 15 mins) to $s \approx 7.5$ Mbp (t = 60 mins). Thus, even in the absence of condensin II, we predict that there is a tendency toward helix formation, which is likely masked in the isotropic ensemble-averaged $P(s)$, especially when the bump in $P(s)$ is not prominent. It is worth noting that both experiments and our calculations show that there is a minor shoulder in the $P(s)$ plots even in the absence of condensin II (Figure 6A).

When only condensin II is present (CAP-H-mAID in the notation used in experiments, where CAP-H stands for chromosome-associated protein H and mAID stands for minimal auxin inducible degron), the amplitudes and the number of peaks increase (Figure 7B) as time progresses. Just as in experiments (see the right panel in Figure 5A in the experimental study by Gibcus et al.[20]), Figure 7B shows that the peak is most prominent at t = 10 min (red), t = 15 min (orange), and t = 30 min (purple). The peak positions shift to larger values of s as the cell cycle progresses toward mitosis. Remarkably, these features are in quantitative agreement with experiments without having to adjust any parameter to fit the experimental data. We compare the $C(s)$ plots at t = 30 min (Figure 7C) and t = 60 min (Figure 7D) in the wild-type (WT), condensin I and condensin II depleted structures. At both time points, the periodicity is more prominent for condensin II-depleted chromosomes than it is when condensin I is depleted. In accordance with experiments, the extent of helix formation appears to be less prominent at t = 60 min compared with t = 30 min.

Helix formation is weaker in HeLa cell chromosomes

It is instructive to compare the s-dependent $C(s)$ for HeLa and DT40 cells (Figure 7D). There are two significant differences. (1) The peak position in $P(s)$ for the chromosomes in the HeLa cell (purple line in Figure 7D) is at a smaller s value compared with the DT40 cells at t = 60 min (blue in Figure 7D). (2) More importantly, the number of peaks, indicating the extent of helix propagation along the genomic distance, is lower in the HeLa cell relative to the DT40 cell. This shows that the extent of helix formation depends on the species and the cell type. Examples of the structural ensemble are given in Figure 7F.

The amplitude of the Fourier transform of $C(s)$ (Figure 7E) for condensin I/II chromosomes at t = 30 and t = 60 min for the WT DT40 and mitotic HeLa cells exhibits prominent peaks for condensin II and DT40 WT cells containing both motors. In contrast, the amplitudes are smaller for HeLa cells and condensin II-depleted DT40 cells, implying that the degree of helix structure is less in HeLa cells. Examples from the structural ensemble are shown in Figure 7F.

RHP in mitotic chromosomes

The precise structural features of mitotic chromosomes have not been firmly established even though several studies[15,54] have shown that they must be helical. That there is an underlying periodicity in the structures is clear from the $C(s)$ as a function of s (Figure 7 and Figure S5). However, from these results we cannot determine whether the helix is left- or right-handed because $C(s) = C(-s)$. For instance, $C(s)$ for a perfect helix is identical regardless of the handedness (Figure S5). Similarly, simulations

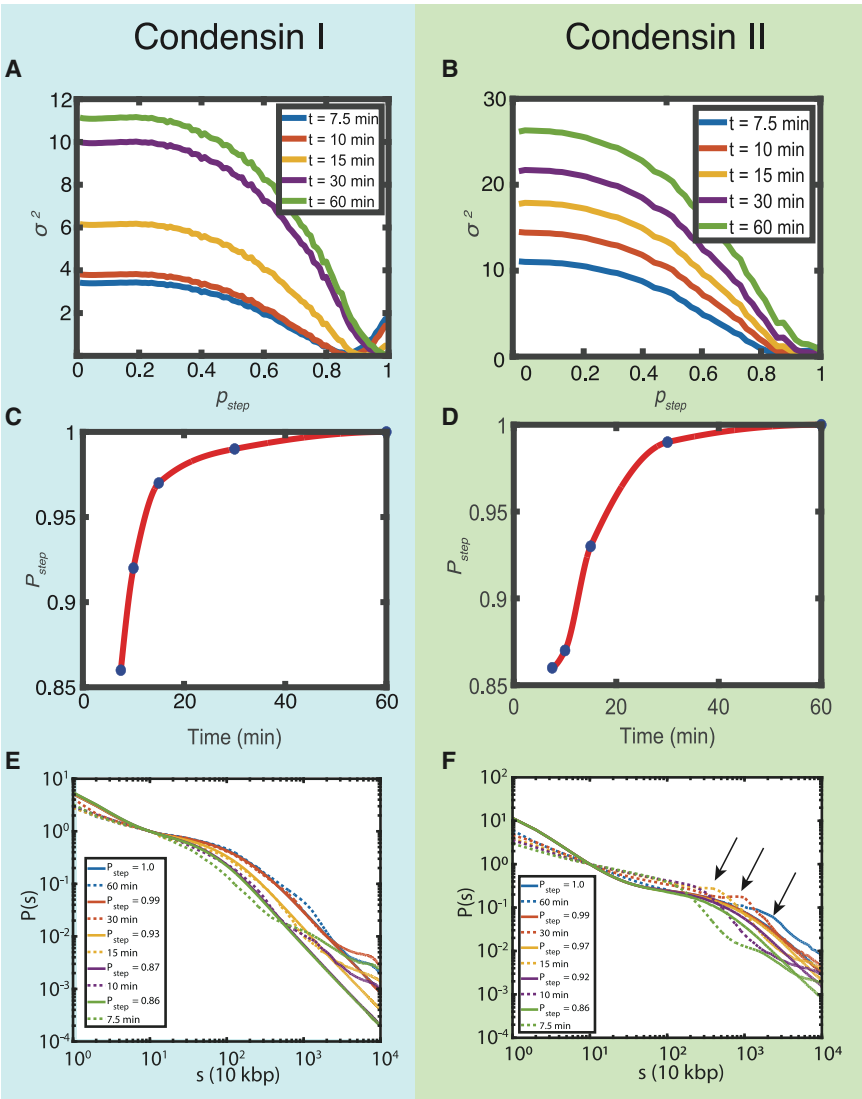

Figure 5. Effect of step size on $P(s)$ for DT40 cells

(A, C, and E) Results for condensin II-depleted cells.

(B, D, and F) Results for condensin I-depleted cells.

(A) Mean-squared error (σ^2; defined in Equation 17 in STAR Methods) between $P(s)$ calculated using A-GRMC and Hi-C at different times for condensin I.

(B) Same as (A) except these are for condensin I-depleted cells.

(C) Optimal values of P_{step} corresponding to the P_{step} that produces the minimum in σ^2 in (A). The lines are from theory, and the dashed curves are experimental data.

(D) Same as (C) except the results are for condensin I-depleted cells.

(E) Comparison of $P(s)$ versus s at different times between the theoretical predictions and experiments for condensin II-depleted cells. The optimal values of P_{step} are given.

(F) Same as (E) except the results are for condensin I-depleted cells. The arrows indicate the bumps in the $P(s)$.

that impose helical conformations and adjust the parameters to fit the $P(s)$ data also cannot determine the handedness unambiguously because $P(s)$ does not contain the information required to make this distinction.

We used the 3D structures to characterize the nature of the mitotic structures. To get insights into plausible arrangements, we first created synthetic structures that are perfectly helical (left or right handed). Not unexpectedly, $C(s)$ for these structures is periodic, with peaks (and valleys) occurring at s values that are integer multiples of the helix pitch, p (measured in megabase pair units; Figure S5). However, they do not match the calculated $C(s)$ from the 3D structures determined using HIPPS. We next generated synthetic structures with RHP by randomly altering the handedness across the entire mitotic chromosomes (see STAR Methods for details). The random feature is controlled by the parameter r, which is zero for a perfectly periodic helix. For $r = 0.01$, the $C(s)$ for the synthetic structures and the results in Figure 7B are similar.

The results in Figure S5 suggest that, in all likelihood, mitotic structures have RHP (a term coined first by Maxwell as reported elsewhere[55,56]) with alterations in handedness occurring randomly. To affirm this possibility, we calculated the helix order parameter[57] expressed in terms of an angle χ, which could be used to extract the local handedness (see supplemental information for definition of χ and the implementation in the context of mitotic chromosomes). Using the 3D coordinates of 1,000 mitotic structures at $t = 30$ min, we calculated the distributions of χ for the ensemble of structures and a single structure. The χ distribution averaged over the 1,000 conformations is broad, with a mean $\chi \approx 0$. Although, for a single conformation, the distribution of χ peaks at $\chi \neq 0$, it is not far from zero. Indeed, the χ distribution in Figure S6F shows that left- and right-handed chiral orders coexist in almost equal numbers in a single conformation. We conclude that each conformation, with a signature of RHP globally, may only have a modest propensity to be left or right handed.

DISCUSSION

We developed a theory based on LE driven by multiple condensin I and condensin II motors to determine the structural changes that occur in chromosomes as the cell cycles from the G2 phase to metaphase. The resulting A-GRMC has two components: (1) a kinetic scheme to determine the dynamics of LE mediated by multiple condensin I/II molecules and (2) a polymer model that takes the location of loop anchors generated by the condensin

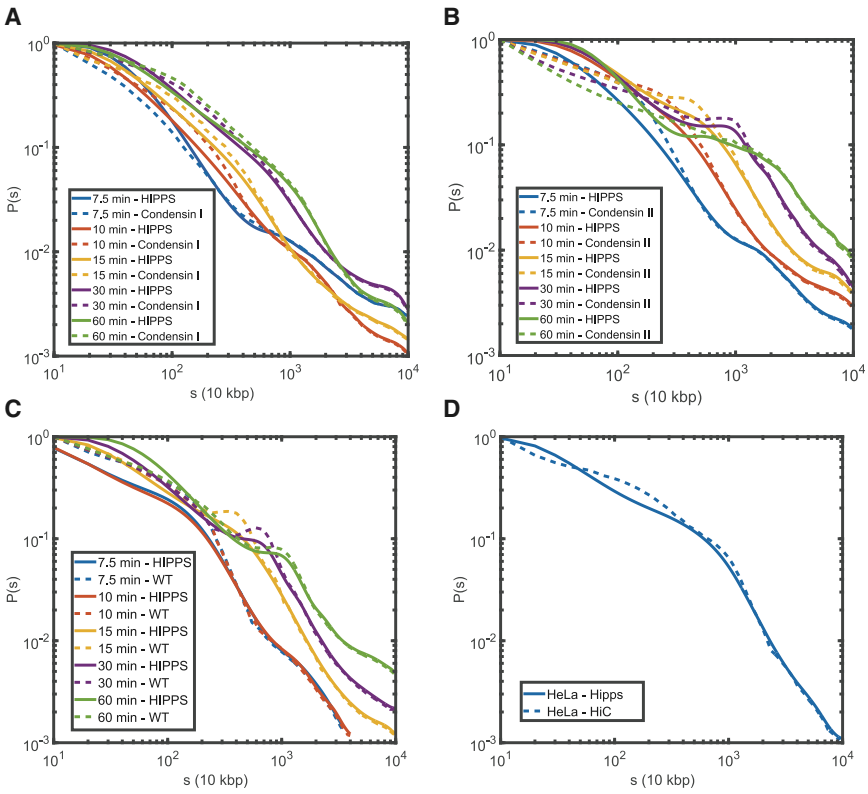

Figure 6. Comparison of calculated $P(s)$ using the HIPPS method (solid lines) with experiments (dashed lines)

(A) $P(s)$ from experiments for DT40 cells with only condensin I (condensin II depleted) at various times compared with the HIPPS calculations.

(B) Same as (A) except the comparison between the HIPPS predictions and experiments correspond to condensin I-depleted cells.

(C) $[P(s), s]$ from experiments for cells with both condensins (WT) at various times compared with the corresponding HIPPS calculations.

(A–C) Results for DT40 cells.

(D) Comparison between HIPPS predictions and experiments for HeLa cells.[47]

motors as input to generate 3D structures of chromosomes. The kinetic scheme is rooted in the scrunching mechanism, discovered first in the context of DNA transcription bubble formation in bacteria,[58] which has recently been invoked to explain the LE mechanism of a single condensin motor.[43,49] Using the A-GRMC together with the results from the HIPPS method, we uantitatively accounted for all experimental data. (1) The calculations based on the A-GRMC accurately predict the behavior of $P(s)$ for mitotic chromosomes in HeLa cells and DT40 chicken cells when condensin II is depleted. (2) The predictions using the A-GRMC are less accurate when only condensin II is present. In particular, the bump in the $P(s)$, whose origin is linked to helix formation in mitotic chromosomes, is not predicted by the A-GRMC theory. (3) Remarkably, the calculations using the HIPPS method predict, with high accuracy, the behavior of $P(s)$ for DT40 cells in the presence of both motors and, upon depletion of the two motors, one at a time. In a sense, the HIPPS method solves the problem by predicting the helical structures with periodicity as the cell cycle progress from interphase to mitosis. (4) We found that the extent of helix formation in mitotic chromosomes depends on the cell type. For HeLa cells, the peak in $P(s)$ is less pronounced compared with DT40 cells, which is also reflected in the angular correlation function ($C(s)$). (5) We find that, even with only condensin I present, there are signatures of weak helix formation in $C(s)$ calculated from the 3D structures. The structures of the mitotic chromosome have the characteristics of RHP, in which the helix handedness changes randomly throughout the chromosome.

Dynamical nature of the chromosomal axis

The cylindrical-shaped mitotic chromosome structure, which emerges naturally in our study, may be thought of as having a scaffold axis, which traces the positions of condensin I and II. The extruded loops, with variable length, are stapled to the scaffold. Because the mitotic chromosome axis is helical, the loops that emanate from the motor proteins trace a helical path. The path traced by the motors is not static because their formation is controlled by at least three timescales that determine the dynamic nature of the helical axis. (1) One is the average LE time. Using the mean loop length for condensin I ($\approx$ 25 kbp) and 150 kbp for condensin II (Figure 4A) and the LE velocity ($\approx$ 1,500 bp/s) for extrusion by a single motor, the extrusion time is 200 s for condensin I and 1,000 s for condensin II. When multiple motors are involved, the time increases by an order of magnitude (Figure 4A). (2) The lifetimes of bound condensins are estimated to be 120 s and 360 s for condensin I and condensin II, respectively. (3) The overall transition time to go from G2 phase to prometaphase is about 30 min in DT40 cells. The first two timescales are less than the cell cycle time, which implies that the motors attach and detach multiple times as the cells transition from G2 to prometaphase. This implies that the loops must be dynamic and that, more importantly, the scaffold is unlikely to be static. Only by averaging over many realizations does an ensemble-averaged backbone structure with possibly complicated helical arrangement (see below) emerge.

Arrangement of loops

Microscopy experiments[59,60] have suggested that the shape of the chromosome is cylindrical, with the condensin and topoisomerase molecules forming a central axis. It is thought that the loops are roughly perpendicular to the putative central axis, which is dynamic, as evidenced by the observed heterogeneity of the structures. Our calculations show that the loops are not arranged in a strictly consecutive non-overlapping fashion because the orientations and the binding sites of the condensins are random and vary from one realization (or cell) to another. The

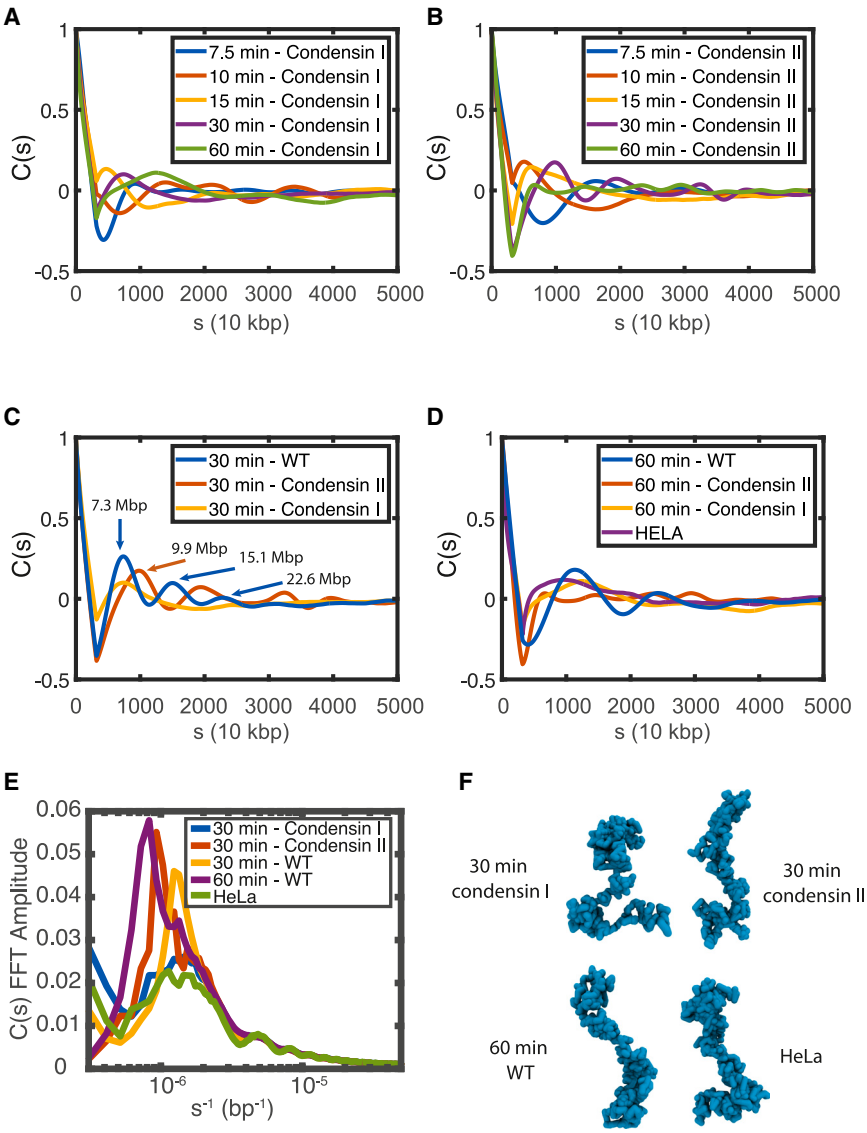

Figure 7. Angular correlation ($C(s)$) as a function of genomic distance at different times

(A) $C(s)$ as a function of s at various times for DT40 cells without condensin II. A peak at $s \approx 5Mb$ with a small amplitude that is most pronounced at t = 15 min (orange line) suggests that condensin I alone induces helix formation but not as much as condensin II.

(B) $C(s)$ as a function of time for condensin II chromosomes (condensin I-depleted) in DT40 cells. The periodicity (roughly 10 Mbs), especially at t = 30 min, is a signature of helix formation.

(C) Comparison of $C(s)$ versus s for WT (blue) condensin I-depleted cells (orange) and condensin II-depleted (red) DT40 cells at t = 30 min.

(D) Same as (C) except these correspond to t = 60 min. Also shown is $P(s)$ versus s for HeLa cells (violet), which illustrates less prominent helicity.

(E) Fourier transform of $C(s)$ as a function of s^{-1} shows that, in the amplitude spectrum, condensin II chromosomes demonstrate stronger peaks compared with condensin I chromosomes. The peaks for HeLa cells are weaker peaks compared with DT40 cells.

(F) Example structures constructed from HIPPS for t = 30 min condensin I/II along with WT DT40 cells at t = 60 min and HeLa cells. The structures show that the HIPPS method accurately predicts the expected conformal features in the mitotic chromosome.

combination of nested loops and Z-loops creates structures that bear some resemblance to polymer bottle brushes, except that the central axis dynamically changes because the motors bind and unbind several times during the cell cycle.

Roles of condensin I and condensin II in shaping the mitotic chromosomes

Since the pioneering discovery of condensin II,[53] there have been several studies[28,52,61] that have probed the differing roles these motors play in formation of mitotic chromosomes. Although condensin I and II load onto chromosomes independently, with the former gaining access only after breakdown of the nuclear envelope, both are required for mitotic chromosome assembly. It has been suggested[23] that condensin II imparts rigidity to the chromosomal axis, whereas condensin I enables lateral compaction.

The A-GRMC simulations show that condensin II extrudes long loops (by a factor of six) compared with condensin I. This implies that the establishment of long-range contacts between distant loci requires condensin II, whereas condensin I assists with generation of short-ranged contacts. Coincidentally, the short-range contacts occur on length scales that are characteristic of TAD sizes, whereas the genomic size of long-range contacts is associated with compartment sizes. The 3D structures generated by the HIPPS method shows (Figure 7B) an emergent length scale at $s \approx 10$ Mbp in $C(s)$, which coincides with the peak in $P(s)$ at t = 30 min (Figure 6B). To the extent that rigidity arises from the periodic structure, we surmise that condensin II might determine the backbone stiffness.[52]

RHP

Although the radial loop model, extracted from micrographs,[15] seems to suggest that mitotic chromosomes are left handed, this issue has not been settled and has come to focus in a recent insightful imaging study.[40] The authors propose that the helix is best described as a periodic helix (or tendril) perversion (PHP). The PHP is a perfect repeat of monomer units. Each unit consists of one left- and one right-handed helix. For structures with PHP, $C(s)$ is shown in Figure S5 for synthetically generated structures. Comparison of $C(s)$ predicted by the HIPPS method and $C(s)$ for structures with PHP shows qualitative differences. Although we established that the HIPPS method, which uses Hi-C data as

input, quantitatively reproduces $P(s)$ at all time points, the consequences of ensemble averaging and lack of error estimates in the Hi-C experiments make it hard to assess the reliability of drawing firm conclusions about the details of mitotic structures. Therefore, additional super-resolution imaging studies, which can determine structures at the single-chromosome level, will be required to definitely address the nature of helix perversion in mitotic chromosomes. That nature would choose helix perversion might be related to stability, which was already noted by Darwin[62] in the context of creeping plants.

The conclusions reached here concerning RHP are not inconsistent with a recent study,[63] which used an entirely different approach. In that study, Hi-C data for mitotic chromosomes were used as input to determine the parameters of an assumed energy function using the maximum entropy method. Most interestingly, the authors found that the structures, obtained by simulations of the energy functions with learned parameters obtained by fitting to the Hi-C data, showed that the overall shape of the mitotic chromosomes is cylindrical, consisting of a mixture of left- and right-handed helices, implying that chiral symmetry is spontaneously broken. The resulting structures, on an average, are likely to be similar to our findings.

In summary, we have introduced a model that could be a reasonable starting point for elucidating the mechanism for predicting multiple condensin-driven structural changes that occur during the mitotic cycle. In combination with the HIPPS method, we have derived plausible structures of mitotic chromosomes. Despite some success, the difficult problem of cooperation between hundreds of condensin (and other) motors remains a daunting challenge.

Limitations of the study

The most glaring weakness of our study is that the calculated $P(s)$ using the A-GRMC model in the presence of only condension II (condension I is depleted) is not in quantitative agreement with experimental measurements. The chromosome structure, upon condensin I depletion, does have a cylindrical shape, but the bump in $P(s)$ that moves to larger values of s as the cell cycle proceeds toward mitosis is not captured. Although we quantitatively reproduced the experimental $P(s)$ using the HIPPS method, it does not reveal the mechanism by which multiple condensin II motors extrude long loops to generate the RHP structures. The differences in the $P(s)$ obtained upon depletion of condensin I (condensin II) suggests that there could be subtle but important differences in the LE mechanism employed by the two motors even though their structures, except for the non-SMC (structural maintenance of chromosomes) parts, are similar.

STAR★METHODS

Detailed methods are provided in the online version of this paper and include the following:

SUPPLEMENTAL INFORMATION

Supplemental information can be found online at https://doi.org/10.1016/j.celrep.2023.112348.

ACKNOWLEDGMENTS

We thank Kiran Kumari, Xin Li, and Sucheol Shin for useful discussions. This work was supported by a grant from the National Science Foundation (CHE19-00033) and the Welch Foundation through the Collie-Welch Chair (F-0019).

AUTHOR CONTRIBUTIONS

A.D. and D.T. designed the research. A.D., G.S., and R.T. performed the research. All authors analyzed the data. A.D. and D.T. wrote the paper with input from G.S. and R.T.

DECLARATION OF INTERESTS

The authors declare no competing interests.

INCLUSION AND DIVERSITY

We support inclusive, diverse, and equitable conduct of research.

Received: June 29, 2022
Revised: November 10, 2022
Accepted: March 21, 2023

REFERENCES

1. Dekker, J., Rippe, K., Dekker, M., and Kleckner, N. (2002). Capturing chromosome conformation. Science *295*, 1306–1311.
2. Dixon, J.R., Selvaraj, S., Yue, F., Kim, A., Li, Y., Shen, Y., Hu, M., Liu, J.S., and Ren, B. (2012). Topological domains in mammalian genomes identified by analysis of chromatin interactions. Nature *485*, 376–380.
3. Hsieh, T.-H.S., Weiner, A., Lajoie, B., Dekker, J., Friedman, N., and Rando, O.J. (2015). Mapping nucleosome resolution chromosome folding in yeast by micro-c. Cell *162*, 108–119.
4. Lieberman-Aiden, E., Van Berkum, N.L., Williams, L., Imakaev, M., Ragoczy, T., Telling, A., Amit, I., Lajoie, B.R., Sabo, P.J., Dorschner, M.O., et al. (2009). Comprehensive mapping of long-range interactions reveals folding principles of the human genome. Science *326*, 289–293.
5. Rao, S.S.P., Huntley, M.H., Durand, N.C., Stamenova, E.K., Bochkov, I.D., Robinson, J.T., Sanborn, A.L., Machol, I., Omer, A.D., Lander, E.S., and

Aiden, E.L. (2014). A 3d map of the human genome at kilobase resolution reveals principles of chromatin looping. Cell *159*, 1665–1680.

6. Van Steensel, B., and Dekker, J. (2010). Genomics tools for unraveling chromosome architecture. Nat. Biotechnol. *28*, 1089–1095.
7. Belaghzal, H., Borrman, T., Stephens, A.D., Lafontaine, D.L., Venev, S.V., Weng, Z., Marko, J.F., and Dekker, J. (2021). Liquid chromatin hi-c characterizes compartment-dependent chromatin interaction dynamics. Nat. Genet. *53*, 367–378.
8. Brackley, C.A., and Marenduzzo, D. (2020). Bridging-induced microphase separation: photobleaching experiments, chromatin domains and the need for active reactions. Brief. Funct. Genomics *19*, 111–118.
9. Jost, D., Carrivain, P., Cavalli, G., and Vaillant, C. (2014). Modeling epigenome folding: formation and dynamics of topologically associated chromatin domains. Nucleic Acids Res. *42*, 9553–9561.
10. Shi, G., Liu, L., Hyeon, C., and Thirumalai, D. (2018). Interphase human chromosome exhibits out of equilibrium glassy dynamics. Nat. Commun. *9*, 3161.
11. Cremer, T., and Cremer, M. (2010). Chromosome territories. Cold Spring Harb. Perspect. Biol. *2*, a003889.
12. Haaf, T., and Schmid, M. (1991). Chromosome topology in mammalian interphase nuclei. Exp. Cell Res. *192*, 325–332.
13. Manders, E.M., Kimura, H., and Cook, P.R. (1999). Direct imaging of dna in living cells reveals the dynamics of chromosome formation. J. Cell Biol. *144*, 813–821.
14. Marko, J.F. (2008). Micromechanical studies of mitotic chromosomes. Chromosome Res. *16*, 469–497.
15. Marsden, M.P., and Laemmli, U.K. (1979). Metaphase chromosome structure: evidence for a radial loop model. Cell *17*, 849–858.
16. Naumova, N., Imakaev, M., Fudenberg, G., Zhan, Y., Lajoie, B.R., Mirny, L.A., and Dekker, J. (2013). Organization of the mitotic chromosome. Science *342*, 948–953.
17. Paulson, J.R., and Laemmli, U.K. (1977). The structure of histone-depleted metaphase chromosomes. Cell *12*, 817–828.
18. Yokota, H., Van Den Engh, G., Hearst, J.E., Sachs, R.K., and Trask, B.J. (1995). Evidence for the organization of chromatin in megabase pair-sized loops arranged along a random walk path in the human g0/g1 interphase nucleus. J. Cell Biol. *130*, 1239–1249.
19. Paulson, J.R., Hudson, D.F., Cisneros-Soberanis, F., and Earnshaw, W.C. (2021). Mitotic chromosomes. Semin. Cell Dev. Biol. *117*, 7–29.
20. Gibcus, J.H., Samejima, K., Goloborodko, A., Samejima, I., Naumova, N., Nuebler, J., Kanemaki, M.T., Xie, L., Paulson, J.R., Earnshaw, W.C., et al. (2018). A pathway for mitotic chromosome formation. Science *359*, eaao6135.
21. Dej, K.J., Ahn, C., and Orr-Weaver, T.L. (2004). Mutations in the drosophila condensin subunit dcap-g: defining the role of condensin for chromosome condensation in mitosis and gene expression in interphase. Genetics *168*, 895–906.
22. Gerlich, D., Hirota, T., Koch, B., Peters, J.-M., and Ellenberg, J. (2006). Condensin i stabilizes chromosomes mechanically through a dynamic interaction in live cells. Curr. Biol. *16*, 333–344.
23. Green, L.C., Kalitsis, P., Chang, T.M., Cipetic, M., Kim, J.H., Marshall, O., Turnbull, L., Whitchurch, C.B., Vagnarelli, P., Samejima, K., et al. (2012). Contrasting roles of condensin i and condensin ii in mitotic chromosome formation. J. Cell Sci. *125*, 1591–1604.
24. Hagstrom, K.A., Holmes, V.F., Cozzarelli, N.R., and Meyer, B.J. (2002). C. elegans condensin promotes mitotic chromosome architecture, centromere organization, and sister chromatid segregation during mitosis and meiosis. Genes Dev. *16*, 729–742.
25. Hirano, T., and Mitchison, T.J. (1994). A heterodimeric coiled-coil protein required for mitotic chromosome condensation in vitro. Cell *79*, 449–458.
26. Hudson, D.F., Vagnarelli, P., Gassmann, R., and Earnshaw, W.C. (2003). Condensin is required for nonhistone protein assembly and structural integrity of vertebrate mitotic chromosomes. Dev. Cell *5*, 323–336.
27. Oliveira, R.A., Coelho, P.A., and Sunkel, C.E. (2005). The condensin i subunit barren/cap-h is essential for the structural integrity of centromeric heterochromatin during mitosis. Mol. Cell Biol. *25*, 8971–8984.
28. Ono, T., Fang, Y., Spector, D.L., and Hirano, T. (2004). Spatial and temporal regulation of condensins i and ii in mitotic chromosome assembly in human cells. Mol. Biol. Cell *15*, 3296–3308.
29. Siddiqui, N.U., Rusyniak, S., Hasenkampf, C.A., and Riggs, C.D. (2006). Disruption of the arabidopsis smc4 gene, atcap-c, compromises gametogenesis and embryogenesis. Planta *223*, 990–997.
30. Strunnikov, A.V., Hogan, E., and Koshland, D. (1995). Smc2, a saccharomyces cerevisiae gene essential for chromosome segregation and condensation, defines a subgroup within the smc family. Genes Dev. *9*, 587–599.
31. Earnshaw, W.C., and Laemmli, U.K. (1983). Architecture of metaphase chromosomes and chromosome scaffolds. J. Cell Biol. *96*, 84–93.
32. Paturej, J., Sheiko, S.S., Panyukov, S., and Rubinstein, M. (2016). Molecular structure of bottlebrush polymers in melts. Sci. Adv. *2*, e1601478.
33. Pienta, K.J., and Coffey, D.S. (1984). A structural analysis of the role of the nuclear matrix and dna loops in the organization of the nucleus and chromosome. J. Cell Sci. Suppl. *1984*, 123–135.
34. Boy de la Tour, E., and Laemmli, U.K. (1988). The metaphase scaffold is helically folded: sister chromatids have predominantly opposite helical handedness. Cell *55*, 937–944.
35. Earnshaw, W.C. (1988). Mitotic chromosome structure. Bioessays *9*, 147–150.
36. Kuwada, Y. (1939). Chromosome structure a critical review. Cytologia *10*, 213–256.
37. Ohnuki, Y. (1968). Structure of chromosomes. Chromosoma *25*, 402–428.
38. Rattner, J.B., and Lin, C.C. (1985). Radial loops and helical coils coexist in metaphase chromosomes. Cell *42*, 291–296.
39. Woodcock, C.L., Frado, L.-L., and Rattner, J.B. (1984). The higher-order structure of chromatin: evidence for a helical ribbon arrangement. J. Cell Biol. *99*, 42–52.
40. Chu, L., Liang, Z., Mukhina, M., Fisher, J., Vincenten, N., Zhang, Z., Hutchinson, J., Zickler, D., and Kleckner, N. (2020). The 3d topography of mitotic chromosomes. Mol. Cell *79*, 902–916.e6.
41. Ganji, M., Shaltiel, I.A., Bisht, S., Kim, E., Kalichava, A., Haering, C.H., and Dekker, C. (2018). Real-time imaging of dna loop extrusion by condensin. Science *360*, 102–105.
42. Kong, M., Cutts, E.E., Pan, D., Beuron, F., Kaliyappan, T., Xue, C., Morris, E.P., Musacchio, A., Vannini, A., and Greene, E.C. (2020). Human condensin i and ii drive extensive atp-dependent compaction of nucleosome-bound dna. Mol. Cell *79*, 99–114.e9.
43. Takaki, R., Dey, A., Shi, G., and Thirumalai, D. (2021). Theory and simulations of condensin mediated loop extrusion in dna. Nat. Commun. *12*, 1–10.
44. Bryngelson, J., and Thirumalai, D. (1996). Internal constraints induce localization in an isolated polymer molecule. Phys. Rev. Lett. *76*, 542–545.
45. Rouse, P.E., Jr. (1953). A theory of the linear viscoelastic properties of dilute solutions of coiling polymers. J. Chem. Phys. *21*, 1272–1280.
46. Shi, G., and Thirumalai, D. (2019). Conformational heterogeneity in human interphase chromosome organization reconciles the fish and hi-c paradox. Nat. Commun. *10*, 1–10.
47. Abramo, K., Valton, A.-L., Venev, S.V., Ozadam, H., Fox, A.N., and Dekker, J. (2019). A chromosome folding intermediate at the condensin-to-cohesin transition during telophase. Nat. Cell Biol. *21*, 1393–1402.
48. Shi, G., and Thirumalai, D. (2021). From hi-c contact map to three-dimensional organization of interphase human chromosomes. Phys. Rev. X *11*, 011051–011077.

49. Ryu, J.-K., Katan, A.J., van der Sluis, E.O., Wisse, T., de Groot, R., Haering, C.H., and Dekker, C. (2020). The condensin holocomplex cycles dynamically between open and collapsed states. Nat. Struct. Mol. Biol. *27*, 1134–1141.

50. Golfier, S., Quail, T., Kimura, H., and Brugués, J. (2020). Cohesin and condensin extrude dna loops in a cell cycle-dependent manner. Elife *9*, e53885.

51. Banigan, E.J., and Mirny, L.A. (2020). The interplay between asymmetric and symmetric dna loop extrusion. Elife *9*, e63528.

52. Hirota, T., Gerlich, D., Koch, B., Ellenberg, J., and Peters, J.-M. (2004). Distinct functions of condensin i and II in mitotic chromosome assembly. J. Cell Sci. *117*, 6435–6445.

53. Ono, T., Losada, A., Hirano, M., Myers, M.P., Neuwald, A.F., and Hirano, T. (2003). Differential contributions of condensin i and condensin II to mitotic chromosome architecture in vertebrate cells. Cell *115*, 109–121.

54. Ohnuki, Y. (1965). Demonstration of the spiral structure of human chromosomes. Nature *208*, 916–917.

55. Goriely, A., and Tabor, M. (1998). Spontaneous helix hand reversal and tendril perversion in climbing plants. Phys. Rev. Lett. *80*, 1564–1567.

56. McMillen, T., and Goriely, A. (2002). Tendril perversion in intrinsically curved rods. J. Nonlinear Sci. *12*, 241–281.

57. Moradi, M., Babin, V., Roland, C., Darden, T.A., and Sagui, C. (2009). Conformations and free energy landscapes of polyproline peptides. Proc. Natl. Acad. Sci. USA *106*, 20746–20751.

58. Kapanidis, A.N., Margeat, E., Ho, S.O., Kortkhonjia, E., Weiss, S., and Ebright, R.H. (2006). Initial transcription by rna polymerase proceeds through a dna-scrunching mechanism. Science *314*, 1144–1147.

59. Adolph, K., Cheng, S., Paulson, J., and Laemmli, U. (1977). Isolation of a protein scaffold from mitotic hela cell chromosomes. Proc. Natl. Acad. Sci. *74*, 4937–4941.

60. Samejima, K., Samejima, I., Vagnarelli, P., Ogawa, H., Vargiu, G., Kelly, D.A., de Lima Alves, F., Kerr, A., Green, L.C., Hudson, D.F., et al. (2012). Mitotic chromosomes are compacted laterally by kif4 and condensin and axially by topoisomerase iiα. J. Cell Biol. *199*, 755–770.

61. Hirano, T. (2016). Condensin-based chromosome organization from bacteria to vertebrates. Cell *164*, 847–857.

62. Darwin, C. (1875). The Movements and Habits of Climbing Plants (John Murray).

63. Zhang, B., and Wolynes, P.G. (2016). Shape transitions and chiral symmetry breaking in the energy landscape of the mitotic chromosome. Phys. Rev. Lett. *116*, 248101.

64. Humphrey, W., Dalke, A., and Schulten, K. (1996). Vmd – visual molecular dynamics. J. Mol. Graph. *14*, 33–38.

65. Eastman, P., Swails, J., Chodera, J.D., McGibbon, R.T., Zhao, Y., Beauchamp, K.A., Wang, L.-P., Simmonett, A.C., Harrigan, M.P., Stern, C.D., et al. (2017). Openmm 7: rapid development of high performance algorithms for molecular dynamics. PLoS Comput. Biol. *13*, e1005659.

66. Sanborn, A.L., Rao, S.S.P., Huang, S.-C., Durand, N.C., Huntley, M.H., Jewett, A.I., Bochkov, I.D., Chinnappan, D., Cutkosky, A., Li, J., et al. (2015). Chromatin extrusion explains key features of loop and domain formation in wild-type and engineered genomes. Proc. Natl. Acad. Sci. USA *112*, E6456–E6465.

67. Shi, G., and Thirumalai, D. (2023). A maximum-entropy model to predict 3D structural ensembles of chromatin from pairwise distances with applications to interphase chromosomes and structural variants. Nat. Commun. *14*, 1150.

68. Walther, N., Hossain, M.J., Politi, A.Z., Koch, B., Kueblbeck, M., Ødegård-Fougner, Ø., Lampe, M., and Ellenberg, J. (2018). A quantitative map of human condensins provides new insights into mitotic chromosome architecture. J. Cell Biol. *217*, 2309–2328.

69. Kim, E., Kerssemakers, J., Shaltiel, I.A., Haering, C.H., and Dekker, C. (2020). Dna-loop extruding condensin complexes can traverse one another. Nature *579*, 438–442.

STAR★METHODS

KEY RESOURCES TABLE

REAGENT or RESOURCE	SOURCE	IDENTIFIER
Software and algorithms		
MATLAB	The MathWorks Inc.	MATLAB
VMD	Humphrey et al.[64]	VMD
OpenMM	Eastman et al.[65]	OpenMM
HIPPS	Shi and Thirumalai[48]	https://doi.org/10.5281/zenodo.7531310
A-GRMC	This paper	https://doi.org/10.5281/zenodo.7686350

RESOURCE AVAILABILITY

Lead contact

Further information and requests for resources should be directed to and will be fulfilled by the lead contact, Dave Thirumalai (dave.thirumalai@gmail.com).

Material availability

This study did not require or generate any materials or reagents.

Data and code availability

This theoretical work does not report original data. All original code has been deposited on GitHub. The code to implement the A-GRMC simulation can be accessed at [https://github.com/at-ray-o/LoopExtrusionGRMC]. The code to implement the HIPPS method can be accessed at [https://github.com/anyuzx/HIPPS-DIMES] and is publicly available as of the date of publication. DOIs are listed in the key resources table. Any additional information required to reanalyze or reproduce the work reported in this paper is available from the lead contact upon request.

EXPERIMENTAL MODEL AND SUBJECT DETAILS

No experimental models were used in this study.

METHOD DETAILS

We developed the Active GRMC (A-GRMC) model, which incorporates the collective *active* dynamics of multiple condensin motors in concert with the GRMC model.[44,60]The calculations using the A-GRMC are done in two steps. First, we perform kinetic simulations of loop extrusion (LE) driven by multiple condensin motors to determine the genomic location of loop anchors as a function of time. The motors are the anchor points to which the loops are stapled. Second, the dynamics of LE is used in conjunction with the GRMC to generate chromosome structures, which allowed us to calculate $P(s)$ that can be compared with experimental data. The technical details are given below and further elaborated in the supplemental information (SI).

Loop extrusions (LE) by multiple condensins

The model for multi-condensin loop extrusion is shown schematically in Figure 1. Each condensin complex, belonging to the Structural Maintenance Complex, is modeled as a pair of capture points on the DNA. In accord with the scrunching mechanism,[43,49] we assume that only one of the capture points (depicted as a circle in Figure 1) moves along the DNA while the other point (depicted as a square) is fixed. In other words, each motor performs one-sided loop extrusion. Condensins disengage from the DNA track stochastically with probability, p_{off}, or load onto DNA with probability p_{on}. The direction of loop extrusion along the DNA is random and the mobile point moves processively (takes many steps before disengaging) along the direction of initial orientation. The A-GRMC kinetic simulations are initiated ($t = 0$) with no bound condensins. At later times, the movement of the mobile-point is controlled by the value of the stepping probability, P_{step} (see supplemental information for details). The values of p_{on} and p_{off} are calculated from number of bound condensins (n_b) and total number of condensins (n_t). These quantities have been measured in experiments (see supplemental information (SI) for details).

Kinetic simulations for multi-condensin LE

The kinetic simulations for multi-condensin driven LE is performed in four steps (Figure 1): (1) At $t = 0$ min, the condensin motors are assumed to be in the unbound state. At each time step, individual motor (condensin I or II) binds to the genome with probability p_{on}.

A bound condensin can also disassociate with probability p_{off}. (2) Once the binding and unbinding events are determined, each newly bound condensin is assigned a random orientation for LE, which is unchanged until the condensin disengages from the genome. (3) A bound condensin takes a single LE step with probability, P_{step}, which is set to unity in all the metaphase chromosome calculations, unless specified otherwise. The location of the mobile point after a single LE step is determined by the step size of condensin, which is sampled from the distribution given in the STAR Methods (Equation 4). Results obtained using an alternative step-size distribution is also shown in Figure S1. If the motor encounters another condensin, it pauses (does not take any steps) for a time duration, τ_p. (4) After executing these events, the clock is advanced by one time-step, and the first three steps are repeated. The parameters in the kinetic simulations, listed in Table S5, are determined using the experimental data. The details are in the STAR Methods.

The locations of the condensin heads constitute the scaffold from which loops of various sizes emanate. At each time step, the genome locations of the condensin heads are determined and used in conjunction with GRMC to obtain the chromatin structures.

A-GRMC

The energy function for A-GRMC (Equation 6 in the STAR Methods) has two terms: (1) the chain connectivity, modeled using harmonic bonds, with a spring constant, $k = 3k_BT/b^2$, where b is the locus size, (2) the looping interaction, which is also modeled using harmonic potentials between the two heads of condensin with the same spring constant, as given above. The dynamics of the loops are determined by the kinetic simulation described above and illustrated in Figure 1. The loop anchors that are pinned by the motors serve as the backbone scaffold for the chromosome. At each time-step in the kinetic simulation, the loop anchors are fixed and their positions are known. Thus, the energy function (Equation 6) is fully determined. Given the energy function, the chromosome structures can be generated (see details in the STAR Methods) from which $P(s)$ as a function of s, can be readily calculated (see details in the STAR Methods). Without loss of generality, we use reduced units by setting $k_BT = 1$, and the locus size $b = 1$, which is on the order of a hundred microns in real units.[48]

Each coarse-grained monomer in the A-GRMC represents 10 kbp, which is longer than the persistence length of DNA and likely also the chromatin fiber,[66] justifying the use of the flexible polymer model without any angle potential (Equation 6). Although the fundamental length scale of the loop-extrusion step is comparable to the persistence length of DNA, the total chromosome length is orders of magnitude larger. Therefore, even though the step-size distribution is calculated using the Equation 4 in the STAR Methods, which is derived for semi-flexible polymers, we model the chromosomes as a generalized Rouse polymer.

Hi-C-polymer-physics-structures (HIPPS)

To complement the A-GRMC model, we used the HIPPS method,[48] whose sole input is the measured contact maps from Hi-C experiments. Because the details of the HIPPS method, including its theoretical basis, and applications are given elsewhere,[48,67] here we only provide a brief description. The algorithm implementing HIPPS has three steps: (1) First, the mean contact probability between two loci i and j is used to calculate the average spatial distance between them using polymer physics concepts.[48] In practice, we produced smooth contact maps, C_{ij} from $P(s)$ inferred from the Hi-C experiments. The matrix C_{ij} is then transformed to a distance map. (2) The mean distance matrix between all the loci is used as a constraint to construct the probability distribution of the loci coordinates using the maximum entropy principle. The essential equations in the HIPPS calculations are provided in the STAR Methods. The HIPPS method generates an ensemble of 3D coordinates for the loci using experimental Hi-C map *without* constructing any polymer model. The $P(s)$ versus s plots can be readily calculated from the 3D coordinates. Shi and Thirumalai[48] showed that the HIPPS method is remarkably successful in predicting the 3D structures of all the 23 interphase chromosomes from GM12878 cells.

QUANTIFICATION AND STATISTICAL ANALYSIS

We did not use standard statistical tests for the analysis. The details of all the quantification and statistical analyses are given below.

Estimates of p_{on} and p_{off}

The theory for generating the shape of the mitotic chromosomes is based on the model described in Figure 1 in the main text. Two key parameters needed for the simulation of the Active-Generalized Rouse Model for Chromosomes (A-GRMC) are, p_{on} and p_{off}, which are the probabilities that condensin motors bind and unbind from DNA, respectively. We calculated p_{on} and p_{off} using data from Fluorescence Recovery After Photo (FRAP) experiments[68] for the residence times of condensin I and II bound to chromosomes. Since the mechanisms of the binding-unbinding processes are unknown, we assume that they obey first order kinetics. We assumed that at each step in the simulations condensin binds or unbinds with probability p_{on} and p_{off}, respectively. The average time (in units of the a time step = 1 s - see the next section for an explanation) a single condensin stays bound to a chromosome is,

$$\langle \tau_B \rangle = \sum_{t=1}^{\infty} t \cdot p_{off} \cdot (1 - p_{off})^{(t-1)} = \frac{1}{p_{off}}. \quad \text{(Equation 2)}$$

Since the number of bound (n_b) and unbound (n_u) condensin molecules is relatively constant during mitosis,[68] we assume that they are in equilibrium with each other. Given that the total number of condensins $n_t = n_b + n_u$, consequently at equilibirum,

$$n_u \cdot p_{on} = n_b \cdot p_{off} \Rightarrow p_{on} = \frac{n_b \cdot p_{off}}{n_u}. \quad \text{(Equation 3)}$$

Using the data in Tables S1 and S2, we calculated n_t for both the condensin motors.[68] used diploid HeLa cells whose genome size is $N = 2$ x 7.9 Gbp. Assuming uniform coverage of condensins in 100 Mbps of DNA, $n_t = 403,395 \cdot 100 \cdot 10^6/(2 \cdot 7.9 \cdot 10^9) \approx 2553$ for condensin I and for 100 Mbp of DNA $n_t = 54,219 \cdot 100 \cdot 10^6/(2 \cdot 7.9 \cdot 10^9) \approx 343$ Condensin II. Because n_b for condensin I varies during mitosis, we used the highest value of n_b which is formed during prometaphase (shown in Table S3). Thus, for a 100 Mbps DNA $n_b = 190433 \cdot 100 \cdot 10^6/(2 \cdot 7.9 \cdot 10^9) \approx 1205$ for condensin I. The total number of condensin II molecules remain relatively constant, so we used the average number from Table S4, which leads to $n_b = 33180 \cdot 100 \cdot 10^6/(2 \cdot 7.9 \cdot 10^9) \approx 210$.

We used the average value of bound time $\langle \tau_B \rangle = 120$ s, for condensin I and $\langle \tau_B \rangle = 360$ s, for condensin II. The use of average values did not significantly change any of the results. Using these values in Equation 1 and 2, we calculated p_{on} and p_{off} for condensin I and II.

The parameters, listed in the Table S5 in the supplemental information, show that p_{on} and p_{off} are different for condensin I and II. All the six parameters needed in the A-GRMC simulations are obtained from experiments. It is in this sense that we consider the A-GRMC simulations to be free of parameters. We also varied some of the parameters (τ_P, the pausing time when two motors collide, τ_B, the mean life time of the motors bound to chromatin, and p_{on} and p_{off}) in order to assess their effect on $P(s)$ as a function of the genomic distance, s. The results are shown in Figure S4. The parameters used for the A-GRMC calculation are given in Table S5.

Calculation of the number of steps per second

In an earlier study,[43] we calculated the step-size distribution, $P(L|R)$, for loop-extrusion by assuming that a condensin of length R captures a loop with contour length L. The distribution, $P(L|R)$ is given by,

$$P(L|R) = C \frac{4\pi N\{L\}(R/L)^2}{L\left(1 - (R/L)^2\right)^{9/2}} \exp\left(-\frac{3t\{L\}}{4\left(1 - (R/L)^2\right)}\right), \quad \text{(Equation 4)}$$

where $t\{L\} = 3L/2l_p$ with $l_p = 50\,nm$ is the persistence length of the DNA, and $N\{L\} = \frac{4\alpha^{3/2}e^{\alpha}}{\pi^{3/2}(4+12\alpha^{-1}+15\alpha^{-2})}$ with $\alpha\{L\} = 3t/4$. The normalization constant C is independent of L. The distribution $P(L|R)$ does not have a well-defined mean and variance. Moreover, the Cumulative Density Function (CDF) of $P(L|R)$ cannot be easily calculated, which makes it difficult to sample $P(L|R)$ in simulations. Therefore, we numerically discretized $P(L|R)$ from $0 \leq L \leq 100,000$ nm. We sampled the discretized distribution by linearly interpolating between adjacent points in the CDF.

By using $P(L|R)$, we calculated the number of steps per second required to achieve a loop extrusion (LE) rate of $1,500bp/s$, which is the measured value in single molecule experiments at small external loads. In the experiment[41] the LE rate = $1,500bp/s$ corresponds to 0.3 relative DNA extension. In their paper, the relative extension is defined as the length between the tethers at either end of the DNA divided by the length of unextruded DNA. From Figure 3 in,[41] the length between the tethers is $\approx 4\mu$m. Thus, for 0.3 relative extension, the length of the DNA that is not extruded is $\frac{4}{0.3} = 13.33\mu$m. Given the length of the $\lambda -$ DNA in the experiment is $20\mu m$, the length of the loop is $(20 - 13.33)\mu m \approx 6.7\mu m$.

We found it takes ≈ 9.63 steps using Equation 3, to extrude a loop of length $6.7\mu m$, implying each step extrudes a loop with length $6.7/9.63 \approx 0.695\mu$m. Then, using an LE rate of ≈ 1500 bp/s, and assuming that the average distance between two base-pairs is 0.34 nm, we obtain the stepping rate of condensin as 1500 x 0.34 x $10^{-3}/(0.695\mu\text{m}) \approx 0.73 \approx 1$ step/second.

The step size L is chosen from the distribution Equation 4, where R, the size of condensin, which we take to be 40 nm[43]. We assume that when $P_{step} = 1$, both condensin I and II take one step per second to match the measured 1,500 bp/s LE velocity.[41] In most of the paper, we set $P_{Step} = 1$ and only modulate it to reproduce the experimental $P(s)$ for times, $t = 7.5, 10, 15, 30$ minutes, as the DT40 cell cycle progress.

Following an experimental study,[69] we assume that when there is a collision between different condensin sites on the chromatin (either mobile or fixed), the loop-extrusion is paused for $\tau_P \approx 7$ s. We also varied τ_P to ascertain the impact on $P(s)$ (see Figure S4). After τ_P, the mobile sites are allowed to move through the blocks. In the LE simulations, the chromosome is modeled as a linear track with 100 bp resolution, which is less than the canonical value of the DNA persistence length. On this length scale, DNA is best described as a semi-flexible polymer, making it necessary to use the step-size distribution given in Equation 4. The time-resolution in the simulation is 1 s, and the LE simulations are performed for about 60 min.

$P(s)$ is captured using rouse model

The agreement between the theoretical (A-GRMC) and experimental $P(s)$ is not sensitive to the exact nature of $P(L|R)$. As shown in Figure S1, instead of using Equation 3, we used the $P(L|R)$ derived from $P(R|L)$ where $P(R|L)$ which for a Rouse Chain with length L and monomer size b has the following form,

$$P(L|R) = C \cdot 4\pi R^2 \left(\frac{3}{2\pi \cdot L \cdot b}\right)^{3/2} \exp\left(-\frac{3R^2}{2 \cdot L \cdot b}\right), \quad \text{(Equation 5)}$$

where $C = \frac{b}{6R}\left\{1/\left(1 - \mathrm{Erf}\sqrt{\frac{3R}{2b}}\right)\right\}$ (Figure S1A), where $Erf(x)$ is the error function. Interestingly, the shape of the $P(s)$ curve obtained using Equation 4 is similar to the one obtained with the one obtained using Equation 3.

Calculations of contact map and structures using A-GRMC

Contact map

We first derive an expression for the contact map for a particular choice of loop anchors (the trace of the condensin motors) specified by L. Let $\mathbf{r}_i = (x_i, y_i, z_i)$ be the position of the i^{th} locus. The GRMC energy function associated with the loop conformation is,[44,48]

$$\mathcal{H} = \frac{k}{2}\sum_{i=1}^{N-1}(\mathbf{r}_{i+1} - \mathbf{r}_i)^2 + \frac{k}{2}\sum_{\alpha=1}^{n(L)-1}\left(\mathbf{r}_{L(\alpha+1)} - \mathbf{r}_{L(\alpha)}\right)^2, \quad \text{(Equation 6)}$$

where, $L(\alpha)$ represents the α^{th} loop. The harmonic nature of the GRMC energy function makes it separable, $\mathcal{H} = \mathcal{H}_x + \mathcal{H}_y + \mathcal{H}_z$, where $\mathcal{H}_x = \frac{k}{2}\sum_{i=1}^{N-1}(x_{i+1} - x_i)^2 + \frac{k}{2}\sum_{\alpha=1}^{n(L)-1}(x_{L(\alpha+1)} - x_{L(\alpha)})^2$, which in matrix notation is, $\mathcal{H}_x = \frac{1}{2}\mathbf{x}^T\mathbf{A}\mathbf{x}$. The elements, A_{ij}, are given by,

$$\mathbf{A}_{ij} = \begin{cases} k + \theta_i k, & \text{if } i = j = 1 \text{ or } N, \theta_i = 1 \text{ if i} \in L \text{ and } \theta_i = 0 \text{ otherwise} \\ 2k + 2\theta_i k, & \text{if } i = j \neq 1 \text{ or } N, \theta_i = 1 \text{ if i} \in L \text{ and } \theta_i = 0 \text{ otherwise} \\ -k, & \text{if } |i - j| = 1 \\ -k, & \text{if } i = L(\alpha - 1) \text{ and } j = L(\alpha), \text{or } i = L(\alpha+1) \text{ and } j = L(\alpha) \\ 0, & \text{otherwise} \end{cases} \quad \text{(Equation 7)}$$

In the first two terms of the above equation, θ_i is 1 when i is a loop-base, and is 0 otherwise.

The distribution function is given by,

$$\Psi(\mathbf{r}_N) = \Psi(\mathbf{x}_N)\Psi(\mathbf{y}_N)\Psi(\mathbf{z}_N) \propto exp\left[-\frac{1}{k_B T}\left(\mathcal{H}_x + \mathcal{H}_y + \mathcal{H}_z\right)\right]. \quad \text{(Equation 8)}$$

The property of the multivariate Gaussian distributions allows us to write,

$$\Psi(\mathbf{x}_N) \propto exp\left[-\frac{1}{2k_B T}\mathbf{x}^T\mathbf{A}\mathbf{x}\right]. \quad \text{(Equation 9)}$$

The matrix A cannot be inverted because it is not translationally invariant, which is easily resolved by fixing the first monomer at the origin with the spring constant k. This modifies A, and we can define the matrix $\tilde{\mathbf{A}}_{ij}$ such that,

$$\tilde{\mathbf{A}}_{ij} = \begin{cases} \mathbf{A}_{11} - k \\ \mathbf{A}_{ij}, \end{cases} \quad \text{For all other } i \text{ or } j \quad \text{(Equation 10)}$$

The covariance matrix is the inverse, $\Sigma = \tilde{\mathbf{A}}^{-1}$. Thus, the equilibrium probability distribution of the x-coordinates is a normal distribution, $\tilde{\Psi}(\mathbf{x}_N) \sim \mathcal{N}(0, \Sigma)$. The distribution of the distance along the x axis between each pair of monomers may be written as,

$$P(x_i - x_j = x) \sim \mathcal{N}\left(0, \sigma_{ij}^2\right), \quad \text{(Equation 11)}$$

where $\sigma_{ij}^2 = \Sigma_{ii} + \Sigma_{jj} - 2\Sigma_{ij}$. Our earlier study[46] showed that the distance distribution between the i^{th} and the j^{th} monomer is given by,

$$P(|\mathbf{r}_{ij}| = r) = \sqrt{\frac{2}{\pi}}\frac{1}{\sigma_{ij}}e^{-r^2/2\sigma_{ij}^2}\frac{r^2}{\sigma_{ij}^2}. \quad \text{(Equation 12)}$$

The contact probability between i and j loci is obtained by integrating Equation 12 till a cutoff distance, r_c, which yields,

$$P_{ij} = \int_0^{r_c} dr\sqrt{\frac{2}{\pi}}\frac{1}{\sigma_{ij}}e^{-r^2/2\sigma_{ij}^2}\frac{r^2}{\sigma_{ij}^2} \quad \text{(Equation 13)}$$

$$= \mathrm{Erf}\left(\frac{r_c}{\sqrt{2}\sigma_{ij}}\right) - \sqrt{\frac{2}{\pi}}e^{-r_c^2/2\sigma_{ij}^2}\frac{r_c}{\sigma_{ij}}. \quad \text{(Equation 14)}$$

We used $r_c = b$. By repeating this calculation for all the i and j pairs gives us the contact probabilities for each pair of loci for a given set, L of loop-bases.

Practical implementation

The procedure for the calculation of the loop size and the coordinates of the monomers in the loop are best explained using a single loop between the locus i and $i+k$ on DNA in time T. The total number of steps taken is $N_{step} = \frac{T}{\Delta t}$ where $\Delta t = 1s$. At each time step a

loop of length, l_j, which is sampled using Equation 4 with $R = 40nm$, is extruded. The loop length (in units of 10 kbps) is $k = \sum_j l_j$ where j goes from 1 to N_{step}.

In order to compute the coordinates of all the loci between i and $i+k$, we first calculated the connectivity-matrix A given in Equation 7. The quadratic nature of the energy function associated with the A-GRMC enables us to compute the normal modes of the system. Each coordinate $(i,(i+1),\cdots(i+k))$ is a linear combination of the normal modes. We write $\mathbf{A}$ as $\mathbf{A} = \mathbf{U}^T\cdot\mathbf{D}\cdot\mathbf{U}$, where $\mathbf{D}$ is a diagonal matrix, and $\mathbf{U}$ is the eigenvector of $\mathbf{A}$. Furthermore, we can write $\mathbf{A} = \mathbf{U}^T\cdot\mathbf{D}^{1/2}\cdot\mathbf{I}\cdot\mathbf{D}^{1/2}\cdot\mathbf{U}$, where $\mathbf{I}$ is an identity matrix. Equation 9 can now be rewritten as

$$\Psi(\mathbf{x}_N)\propto exp\left[-\frac{1}{2k_BT}\lambda^T\mathbf{I}\lambda\right], \quad \text{(Equation 15)}$$

where $\lambda = (\mathbf{D}^{1/2}\cdot\mathbf{U}\cdot\mathbf{x})$. Since I is the identity matrix Equation 15 can be separated into N independent $\mathcal{N}(0,1)$ distributions. These are the distributions of the normal mode vectors. We sample each normal mode vector separately from $\mathcal{N}(0,1)$ and use $\mathbf{x} = (\mathbf{D}^{1/2}\cdot\mathbf{U})^{-1}\cdot\lambda$ to generate the coordinates of the loci in the loop connecting i and $i+k$. The same process is repeated for the $\mathbf{y}$ and $\mathbf{z}$ coordinates.

Calculation of $p(s)$

A contact map is constructed by computing P_{ij} for every pair of i,j. The final average CM is computed by averaging over 500 different realizations of loops. From the average CM the probability of contact between two loci separated by a genomic length s, $P(s)$ was computed using,

$$P(s) = \frac{1}{n-s}\sum_{i=1}^{n-s}\mathbf{C}_{i,i+s}, \quad \text{(Equation 16)}$$

where $\mathbf{C}_{i,i+s}$ is the contact frequency between the i^{th} and $(i+s)^{th}$ loci, and the genomic distance s is measured in units of 10 kbps.

To compare between experimental and calculated $P(s)$ versus s, we computed the mean-squared error (σ^2) between the two $P(s)$ curves in the log scale. This is given by,

$$\sigma^2 = \frac{1}{s_{max}}\sum_{s=0}^{s_{max}}\left[\log\left[P(s)_{exp}\right] - \log\left[P(s)_{GRMC}\right]\right]^2. \quad \text{(Equation 17)}$$

A small value of σ^2 implies good agreement between the two $P(s)$ curves.

Contact maps (CMs) generated using A-GRMC simulations are shown in Figure S7A. Just like in experiments,[41] mitotic contact maps are featureless. As a result, there is little distinction between CMs obtained in the presence of only condensin I or condensin II. The only discernible difference is the darker color at the corner of condensin I contact map, which suggests that the contact frequency is smaller. It appears that $P(s)$ is a better metric to visually observe the differences in the contact frequencies.

P_{step} variation

When $P_{step} = 1$ condensin molecules extrude loops at every timestep. If P_{step} is not unity, a step is taken if a random number drawn between $[0,1]$ is less than P_{step}. As explained in the main text, by varying P_{step}, we obtain better agreement with experiments for $P(s)$ for both condensin I/II depleted chromosomes at different time points (Figure 5). Figure S7B also shows that the same optimal P_{step} values for condensin I/II chromosomes could be used even when both types of motors are simultaneously present.

HIPPS calculations

The theoretical basis for the HIPPS method[48] is rooted in the power law that relates the contact probability P_{ij} and the average distance $\langle r_{ij}\rangle$ between loci i and j. The exact relationship between P_{ij} and $\langle r_{ij}\rangle$ is,

$$\langle r_{ij}\rangle = \Lambda P_{ij}^{-1/\alpha}, \quad \text{(Equation 18)}$$

where we use $\Lambda = 1.0$ and $\alpha = 3.0$ for the mitotic chromosomes.[48] The objective is to calculate the joint distribution of the 3D coordinates of the loci, $P(x_i)$, subject to the constraint that the mean pairwise distance is $\langle(x_i - x_j)^2\rangle = \langle r_{ij}^2\rangle$. Since there are potentially an infinite number of $P(x_i)$ distributions that could give the same average pairwise distances, we use the maximum entropy principle to obtain a unique distribution. The maximum entropy distribution, $P^{\text{MaxEnt}}(x_i)$, subject to the constraints associated with the mean squared pairwise spatial distances is given by,

$$P^{\text{MaxEnt}}(\mathbf{x}_i) = \frac{1}{Z}\exp\left(-\sum_{i<j}k_{ij}\|\mathbf{x}_i - \mathbf{x}_j\|^2\right). \quad \text{(Equation 19)}$$

The k_{ij} values are obtained by an optimization procedure. We calculate k_{ij} using an iterative procedure.[48] Let $k_{ij}(t)$ be the value of k_{ij} at the t^{th} iteration. The update is done as,

$$k_{ij}(t+1) = k_{ij}(t) + \frac{r}{\sum_{i<j} r_{ij}^2(t)} \ln \frac{\langle r_{ij}^2(t) \rangle}{\langle r_{ij}^2 \rangle}, \quad \text{(Equation 20)}$$

where r is the learning rate. Full details of the calculation maybe found elsewhere.[48]

Assessing the handedness of mitotic structures

In an effort to understand the helical nature of the mitotic chromosomes, we first computed $C(s)$ for synthetically generated structures. We created helices with 100 Mbps of mitotic chromsomes at 100 Kbps resolution (1,000 loci). The period of the helix (p) is the contour length along the helix needed to complete one turn. This corresponds to the first peak in the $C(s)$ curve (see Figure 7 in the main text). For the synthetic helices, we used a period of 1 Mbps.

In order to elucidate the nature of helix perversion, we introduced a randomness parameter (r) that controls the probability with which the helix changes the handedness. In Figure S5A we show the structures of the helices for different r values. An ideal helix with a definite handedness through out the length of the mitotic chromosome corresponds to $r = 0$. The $C(s)$ for an ideal helix is perfectly periodic (Figure S5B), which is not found in the $C(s)$ calculated using the 3D HIPPS-generated structures (see Figure 7B in the main text). Moreover, $C(s)$ for a structures with Periodic Helix Perversion (PHP), is also periodic (see the purple curve in Figure S5B), and inconsistent with the results in Figure 7B in the main text. In contrast, for $r \neq 0$ (in particular for $r = 0.04$) the $C(s)$ obtained from the synthetic structures resembles the one calculated for condensin I depleted DT40 cells at $t = 30$min (see Figure S5B in the main text), providing the first hint that helix perversion could occur randomly. The qualitative agreement between $C(s)$ calculated using the synthetic and HIPPS-generated structures for $r \neq 0$ suggests that mitotic chromosomes could also have alternating handedness, which was noted recently.[40]

To further quantify the handedness of chromosomes, we used the local helical parameters (χ) introduced by Moradi et al.[57] In Figure S6A, we show the geometric construction for calculating χ. The χ parameter depends on the period of the helix. For a helix with period p, $\overrightarrow{AB}$ and $\overrightarrow{CD}$ are the vectors between the i^{th} and $(i+p/2)^{th}$ centers, and $(i+p/4)^{th}$ and $(i+3p/4)^{th}$ centers, respectively. The vector $\overrightarrow{EF}$ connects the midpoints of $\overrightarrow{AB}$ and $\overrightarrow{CD}$. Using these vectors, χ is defined as the dot product of the unit vector along $\overrightarrow{EF}$ with the unit vector along $\overrightarrow{AB} \times \overrightarrow{CD}$. We computed χ along the whole structure for different values of i. For an ideal right handed helix, the distribution of χ is peaked at 1. Conversely for an ideal left handed helix $\overrightarrow{AB} \times \overrightarrow{CD}$ will always point away from $\overrightarrow{EF}$, and the distribution of χ is peaked at -1.

We computed χ for the structures with $r = 0.01$ and $r = 0.04$ (Figures S6C and S6D). The distribution of χ for $r = 0.01$ has peaks at -1 and 1 in addition to 0. This implies that there are both left and right handed helices. At $r = 0.04$, which produces $C(s)$ that resembles the one shown in Figure 7A in the main text using 3D structures, the peaks at -1 and 1 are lost. The distribution peaks at $\chi = 0$. At $r = 0.04$ the $C(s)$ graphs shows evidence of periodicity, but the helix is neither left or right handed but is a mixture of the two. This would correspond to helix perversion with the handedness switching randomly across the structure.

Finally, we calculated the distribution of χ using the 1,000 structures calculated from HIPPS in condensin II chromosomes at $t = 30$ min (Figure S6E). For these calculations, we used the period $p = 9.9$ Mbps, corresponding to the first peak in the $C(s)$ curve (Figure 7A in the main text). The HIPPS calculations suggest that the entire ensemble of chromosomes could consist of a mixture of left and right handed helices, which is consistent with the conclusions reached previously.[63] When we plot the distribution of χ for a single HIPPS structure in condensin II chromosomes at $t = 30$ min (Figure S6F), we find that there is a modest bias toward $\chi < 0$. This particular structure has hints of being slightly left handed. Thus, mitotic chromosomes in general could have alternating handedness in a single structure, with possible bias toward helices with either handedness.